Journal of Materials Chemistry A

Accepted Manuscript

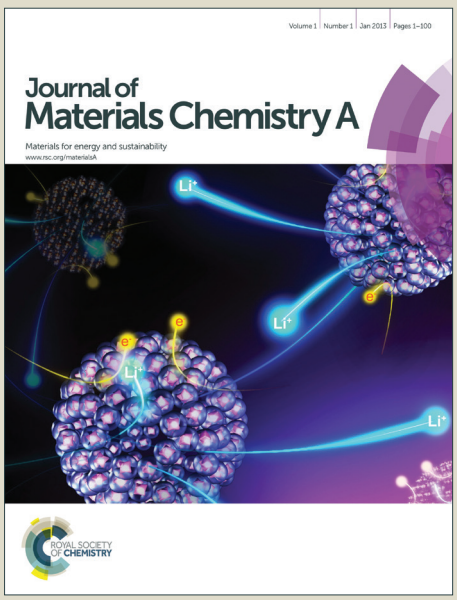

ROYAL SOCIETY OF CHEMISTRY

www.rsc.org/materialsA

A Study of the Superior Electrochemical Performances of 3 nm SnO_2 Nanoparticles Supported by Graphene

*Yu Chen, Bohang Song, Rebecca Meiting Chen, Li Lu, and Junmin Xue**

[*] Yu Chen,[+] Rebecca Meiting Chen, Dr. Junmin Xue

Department of Materials Science and Engineering,

National University of Singapore, Singapore, 117576

E-mail: msexuejm@nus.edu.sg

Bohang Song,[+] Prof. Li Lu

Department of Mechanical Engineering,

National University of Singapore, Singapore, 117576

[+] These authors contributed equally to this work.

Abstract

Owing to the discovery of its new reaction mechanism towards lithium, SnO_2 has recently regained the attention from scientific field as a promising potential anode material. A theoretical capacity of 1494 $mAh \cdot g^{-1}$ can be reached provided that SnO_2 particles are reduced to ultra-small sizes. In addition, other two important aspects, namely cyclic stability and power density, can also be greatly enhanced by applying SnO_2 particles with appropriate dimensions. Therefore, size controlling of SnO_2 naonparticles is critical for their applications in lithium ion batteries (LIBs). In this work, SnO_2 nanoparticles with an average diameter of 3 nm are decorated on graphene nanosheets. Owing to the small sizes of SnO_2 nanoparticles and the electronic conductive graphene network, anode consisting of SnO_2 and graphene (SnO_2/G) delivers a high first reversible capacity of 1239 $mAh \cdot g^{-1}$ at an initial current density of 0.1 $A \cdot g^{-1}$ and a surprisingly 574 $mAh \cdot g^{-1}$ charge capacity under an exceptional high current density of 10 $A \cdot g^{-1}$. Meanwhile, superior cycleability is also

achieved in view of increasing reversible capacity up to 1813 $mAh \cdot g^{-1}$ after over 1000 cycles under a high current density of 2 $A \cdot g^{-1}$. Such stunning performance is carefully studied with various characterization techniques, including electrochemical measurements, TEM, and ex-situ XRD. The high reversible capacity of SnO_2/G is attributed to the 3nm-sized SnO_2 nanoparticles, which almost doubled the theoretical capacity of the oxide. Besides, the excellent performance under high current densities is ascribed to the enhanced lithium and electron diffusion, resulting from the significantly shortened lithium diffusion length within each SnO_2 particle and the conductive graphene network, respectively. In addition, the prominent increment in reversible capacity upon cycling is understood by the increasing number of active lithium storage sites and polymeric gel-like film formation during the prolonged charge/discharge process.

Introduction

To meet the requirements of portable electronics and electric vehicles, the development of the next generation of lithium ion batteries (LIBs) with both high energy density and excellent power density has been an urgent task.[1, 2] Graphite, despite of its great success as the anode of LIBs in the past two decades, has been proven to be unsuitable for advanced applications due to its low theoretical capacity (372 $mAh \cdot g^{-1}$) and poor performance under high current densities.[3] Owing to its relatively high theoretical capacity, natural abundance, and environmental benignity, SnO_2 has been considered as a potential anode material. SnO_2 reacts with lithium through a two-step reaction:4

$$SnO_2 + 4Li^+ + 4e^- \leftrightarrow Sn + 2Li_2O \quad (1)$$

$$Sn + xLi^+ + xe^- \leftrightarrow Li_xSn \ (0 \leqslant x \leqslant 4.4) \quad (2)$$

It has been reported that only the alloying reaction (equation 2) is reversible for bulk SnO_2. As a consequence, the theoretical capacity of SnO_2 has been widely accepted to be 782 $mAh \cdot g^{-1}$ for a long period since the first discovery of SnO_2 as an anode material back in 1997.[5] This value was outperformed by transition metal oxides which were discovered as LIBs' anode materials in 2000,[6] including Fe_3O_4, Fe_2O_3, MnO_2,

Co_3O_4, with higher theoretical capacities ranging from 890 to 1232 $mAh \cdot g^{-1}$.[7-10] However, very recent studies reported that the conversion reaction of equation 1 can also be reversible when the SnO_2 particles are reduced to ultra-small size.[11-13] As a result, SnO_2 is able to reach a theoretical capacity of 1494 $mAh \cdot g^{-1}$, which is over 4 times of that of graphite and higher than those of the transition metal oxides.[14] Such high capacity makes SnO_2 among the several top available candidates for potential anode materials. Besides the high capacity, ultra small SnO_2 nanoparticles are also beneficial to accommodate the volume change accompanied by the lithium insertion/removal and enhance the rate of lithium insertion/removal, ensuring a more stable cycle stability and better performance at high charging current.[15, 16] Therefore, much attention has been paid on developing ultra small SnO_2 nanoparticles and their composites for LIBs' anode applications.[14, 17, 18]

In this work, SnO_2 based composites consisting of 3 nm SnO_2 ultra small nanoparticles and graphene nanosheets were synthesized for potential LIBs' anodes. Graphene has been recognized as an excellent substrate for metal oxide nanoparticles, due to its excellent electric conductivity and mechanical flexibility that can enhance the electron conduction and partially accommodate the volume change of metal oxides, respectively.[19] Besides, the large surface area of graphene can reversibly accommodate large amount of lithium, thus contributing to the overall capacity of the composites.[17] The as-obtained 3 nm SnO_2 nanoparticles attached on graphene composite (SnO_2/G) was electrochemically tested up to an exceptional high current density of 10 $A \cdot g^{-1}$, and subsequently charged/discharged at 2 $A \cdot g^{-1}$ for at least 1000 cycles. Astonishingly, an unexpected high reversible capacity of 574 $mAh \cdot g^{-1}$ was delivered at the current density of 10 $A \cdot g^{-1}$. Furthermore, the capacity climbed to over 1800 $mAh \cdot g^{-1}$ under 2 $A \cdot g^{-1}$ after over 1000 cycles of charge/discharge process. These observed capacity values of our SnO_2/G samples greatly exceed most reported values of SnO_2 anode systems.[17, 18, 20, 21] Therefore, it should be an intriguing work to study the possible mechanism of such superior electrochemical performance. In this work, the electrochemical results and the cycled electrodes were carefully analyzed by

various techniques, including dQ/dV plots in view of different stages of cycling process, together with TEM and ex-situ XRD on cycled electrodes, respectively. Based on the results of our analysis, the ultra-small size of SnO_2 nanoparticles, increasing lithium storage sites on graphene surface resulted from the volume expansion/contraction of SnO_2 nanoparticles, and the formation of polymeric gel-like film are believed to work synergistically in the contribution to the overall superior electrochemical performance of SnO_2/G.

The SnO_2/G anode was synthesized through a one-step hydrothermal method. In a typical synthesis, Tin (IV) chloride pentahydrate, sodium bicarbonate, L-ascorbic acid, and graphene oxide (GO) nanosheets obtained via a modified Hummers method were mixed appropriately and reacted hydrothermally at 150 °C for 6 hours. The small sizes of SnO_2 nanoparticles were achieved by the slow condensation of $Sn(OH)_4$. The detailed procedure of synthesis method is described in experimental section.

Experimental

Materials synthesis

GO was prepared by the oxidation of natural flake graphite powder using a modified Hummers method. In the synthesis of SnO_2/G composite, appropriate amount of GO was firstly dispersed in DI water (30 ml) by ultrasonication. Subsequently, $SnCl_4 \cdot 5H_2O$ (0.47 g) followed by $NaHCO_3$ (0.45 g) were added into the solution. After mixing (30 min) in the aid of magnetic stirring, L-ascorbic acid (0.176 g) was added and the solution was allowed for further mixing (10 min). After that, the mixture was transferred to a Teflon-lined steel autoclave (125 ml) and reacted hydrothermally at 150 °C for 6 hours. The obtained product was collected by centrifuge and washed with DI water several times and freeze dried in vacuum environment.

Characterization

Transmission electron microscope image (TEM) and selected area diffraction (SAED) patterns were examined by a JEOL 100CX instrument using a 300 kV accelerating

voltage. Scanning electron microscope (SEM) and energy-dispersive X-ray spectroscopy (EDS) mapping were collected by a Zeiss Supra 40 FESEM. Powder X-ray diffraction (XRD) patterns were measured by a powder diffractometer (Bruker D8 Advanced Diffractometer System) with Cu Kα (1.5418 Å) source. X-ray photoelectron spectroscopy (XPS) data were obtained by an Axis Ultra DLD X-ray photoelectron spectrometer equipped with an Al Ka X-ray source (1486.6 eV). The thermogravimetric analysis (TGA) was performed under an air flow of 100 mL min^{-1} using Du Pont Instruments TGA 2950 from room temperature to 1000 °C with a heating rate of 10 °C min^{-1}.

Electrochemical measurements

CR2016 coin-type cells were used to test the electrochemical performance of all samples. In the first place, a working electrode was prepared by mixing 70 wt% active materials, 15 wt% carbon black (Super P), and 15 wt% Polyvinylidene Fluoride (PVDF) in n-methyl-2-pyrrolidone (NMP) solution, followed by pasting it onto copper foil before assembly. After drying the electrode at 120 °C over night, its typical loading density is around 1 mg cm^{-2}. All battery cells were carefully assembly using as-prepared electrodes, pure Li foil, separators (Celgard 2500), and electrolyte (1 M $LiPF_6$ in EC : DEC : DMC = 1 : 1 : 1 organic solutions) in an argon-filled glovebox. A fixed voltage window of 0.005 – 3 V vs. Li^0/Li^+ was applied for all electrochemical cycling tests.

Results and discussion

GO was fabricated through a modified Hummers method with characterizations shown in Figure S1. The morphology of the as-synthesized SnO_2/G composite was characterized by TEM and is shown in Figure 1. Figure 1a showed the TEM of SnO_2/G under a low magnification, demonstrating numerous SnO_2 nanoparticles attached on graphene surface. At the early stage of hydrothermal reaction, the oxygen-containing functional groups on the surface of GO acted as anchor points for the decoration of SnO_2 nanoparticles. Subsequently, GO nanosheets were reduced by L-ascorbic acid under elevated temperature, forming SnO_2/G composites.[22] Under a slightly higher magnification as shown in Figure 1b, the uniform attachment of

distinct SnO_2 nanoparticles on graphene nanosheets could be clearly observed. The uniform decoration of SnO_2 nanoparticles could also be proven by even distribution of Sn, O, and C elements shown in the EDS mapping (Figure S2). No obvious aggregation of SnO_2 nanoparticles could be observed, which reduced the risk of pulverization. Under an even higher magnification (Figure 1c), the contour of each SnO_2 nanoparticle could be clearly seen and size of individual SnO_2 particles was measured. According to the size distribution chart shown in Figure S3, the average size of SnO_2 was measured to be around 3 nm. Besides, void spaces were observed in-between each SnO_2 nanoparticles, which was beneficial for the electrolyte penetration during the electrochemical test. Figure 1d showed the high resolution TEM image of SnO_2/G. The lattice fringe of each SnO_2 nanoparticles was clearly observed. The selected area electron diffraction (SAED) of SnO_2/G was shown in Figure S4, which corresponded to the tetragonal SnO_2 structure (JCPDS: 41-1445).

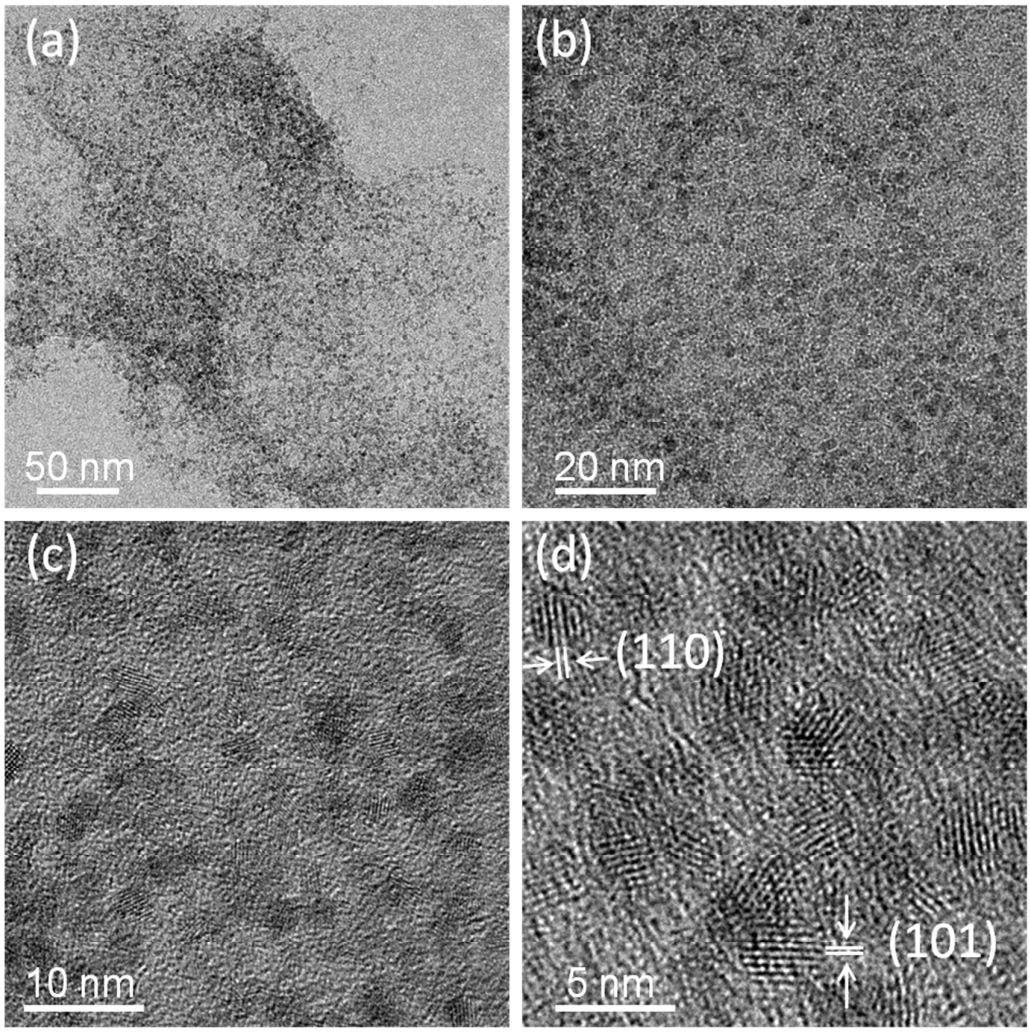

Figure 1. (a-d) TEM images of SnO_2/G under different magnifications.

The XRD patterns of SnO_2/G composite and GO nanosheets were demonstrated in Figure 2a. The distinct and broadened peak located around 10.6° corresponded to an interplanar distance of 8.35 Å for GO nanosheets. Compared with the basal distance of graphite (3.35 Å), such expansion was due to the introduction of oxygen-containing functional groups during the GO formation. As shown in the XRD pattern of SnO_2/G composites, after the decoration of SnO_2 nanoparticles and reduction of GO nanosheets, the peak around 10.6° vanished, indicating negligible stacking of graphene nanosheets. All other peaks were attributed to the tetragonal SnO_2 structure (JCPDS: 41-1445). By applying Scherrer equation, the crystal size of SnO_2 was calculated to be around 3 nm, which was consistent with the result measured from

TEM images. The survey XPS spectrum of SnO_2/G was shown in Figure 2b, confirming the existence of Sn, C, and O elements. Figure 2c showed the XPS spectrum of C 1s from SnO_2/G. Compared with the C 1s obtained from GO (Figure S5), a huge reduction in oxygen content is observed. Specifically, the content of sp^2 bonded carbon at 284.6 eV (C-C) increased from 32.2 to 56.6 %, while the content of epoxy/hydroxyl groups around 286.6 eV decreased from 56.2 to 26.1 %. The reduction of oxygen-containing functional groups was desirable to the partial restoration of electrical conductivity of graphene, thus beneficial to the resultant electrochemical performance. As shown in Figure 2d, the Sn $3d_{5/2}$ and Sn $3d_{3/2}$ were observed to be around 487.3 and 495.7 eV, confirming the formation of SnO_2 nanoparticles.[17] By applying TGA (Figure S6), the SnO_2 content of SnO_2/G composite was determined to be around 55 %. The high proportion of graphene was beneficial to the final electrochemical performance of the composite.

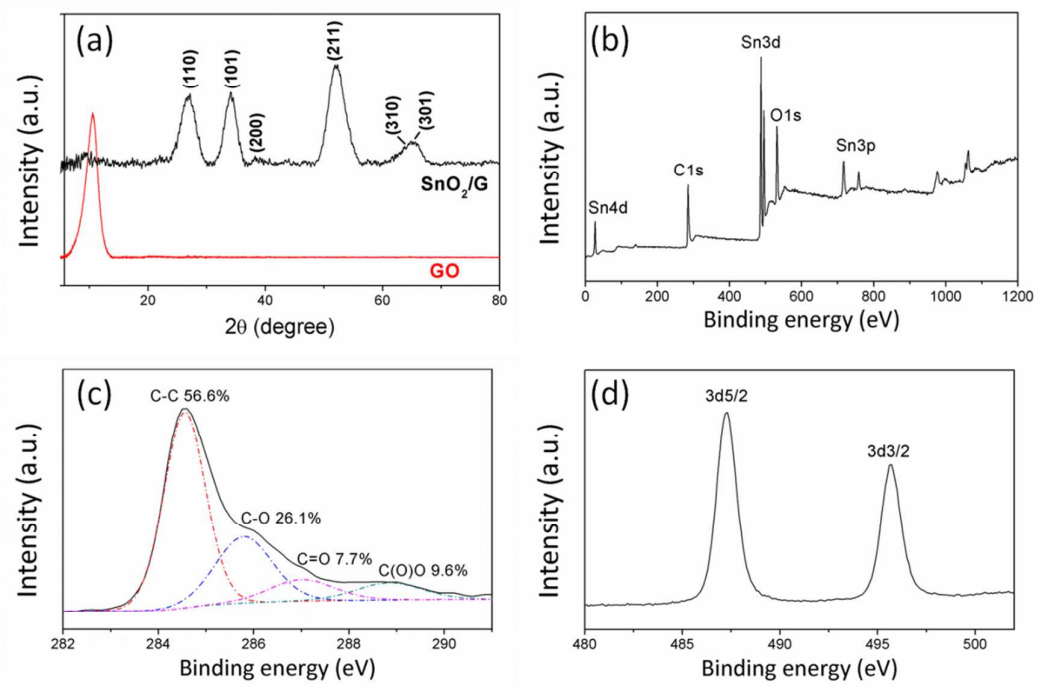

Figure 2. (a) XRD patterns of SnO_2/G (black) and GO (red). (b) Survey XPS spectrum of SnO_2/G. High resolution XPS spectra of (c) C 1s and (d) Sn 3d from SnO_2/G.

The electrochemical performance of SnO_2/G composite as an anode material was investigated under different current densities in a voltage window of 0.005 – 3 V vs. Li/Li^+. As shown in Figure 3a, the first discharge capacity reached 2023 $mAh \cdot g^{-1}$ under a current density of 100 $mA \cdot g^{-1}$, while 1239 $mAh \cdot g^{-1}$ initial charge capacity was achieved as a consequence of the following removal of Li, corresponding to 61.2 % coulombic efficiency. It is important to note that 782 $mAh \cdot g^{-1}$ was a commonly-accepted value as a reversible capacity for bulk SnO_2 solely based on the alloying reaction between Sn and Li (reaction 2). However, our observation of 1239 $mAh \cdot g^{-1}$ reversible capacity was far more beyond such value. The first possible reason for such a high reversible capacity was the ultra-small SnO_2 particles. As reported in several very recent works, compared with their bulk counterpart, ultra-small SnO_2 particles were able to demonstrate partial reversibility in the conversion reaction during cycling (reaction 1).[14, 23, 24] Such phenomenon was supported by the dQ/dV plots of SnO_2/G as shown in Figure S7. Two strong reduction peaks at 1.1 (R_1) and 0.2 V (R_2) were ascribed to decomposition of SnO_2 to Sn and Li_2O composite and alloying reaction to form $Li_{4.4}Sn$, respectively. Correspondingly, two oxidation peaks during delithiation at 0.5 (O_2) and 1.2 V (O_1) were assigned to dealloying of $Li_{4.4}Sn$ and partial decomposition of Li_2O to form SnO_2, respectively. As shown in Figure S7, these peaks (R_1/O_1 and R_2/O_2) continued to appear in the subsequent cycles, proving the reversibility of the corresponding reactions in the following cycles. The second reason for the high capacity of SnO_2 composite was highly related to its graphene content. As observed in many literatures on similar SnO_2/C systems,[25-27] the appearance of carbon content not only significantly improved the specific areas of electrode materials, but also enhanced the reversibility of SEI formation/decomposition. Therefore, large amount of lithium could be reversibly stored on graphene surface, improving the overall capacity of SnO_2/G composite.

To evaluate the rate capability as well as the cycling performance of SnO_2/G composite, the cell was charged/discharged at increasing current densities from 0.5 to 10 $A \cdot g^{-1}$, and then cycled at a constant 2 $A \cdot g^{-1}$ from 131^{th} for 1000 cycles. As represented from Figure 3c, this SnO_2/G composite was able to deliver 908, 882, 854,

780, 716, 653, and 574 mAh·g^{-1} at current densities of 0.5, 1, 2, 4, 6, 8, and 10 A·g^{-1}, respectively. The corresponding charge/discharge curves were shown in Figure 3b. As shown in Figure 3b, compared to the change/discharge curves at low rate 0.5 A·g^{-1}, similar starting points initiating lithiation/delithiation were observed at a much higher current density of 10 A·g^{-1}, indicating significantly low internal resistance in electrode composite. Two advantages based on this unique SnO_2/G composite structure could be regarded as the main reasons for superior rate capability. One desired feature of the SnO_2/G composite was the extremely shortened lithium diffusion path between particle and electrolyte resulted from ultra-small SnO_2 particle. The other reason was that uniformly distributed graphene significantly improves the electronic conductivity within the electrode matrix.

After evaluation of rate capability, the cell was constantly charged/discharged at 2 A·g^{-1} for another 1000 cycles. Most surprisingly, the reversible capacity continuously increased from 890 to 1480 mAh·g^{-1}, and then stabilized around 1450 mAh·g^{-1} for extended cycles. As a matter of fact, the superior rate capability of this SnO_2/G composite as well as increasing reversible capacity exhibited during long-term cycling could be reasonably repeated for other cells. As shown in Figure 3d, another cell fabricated from SnO_2/G was subjected to exactly the same charge/discharge process from 0.5 to 10 A·g^{-1}. A reversible capacity of 1813 mAh·g^{-1} after 1180 cycles at 2 A·g^{-1} was achieved in this case. Such a high capacity is far beyond the normally-observed values in SnO_2-based anode systems.[28, 29]

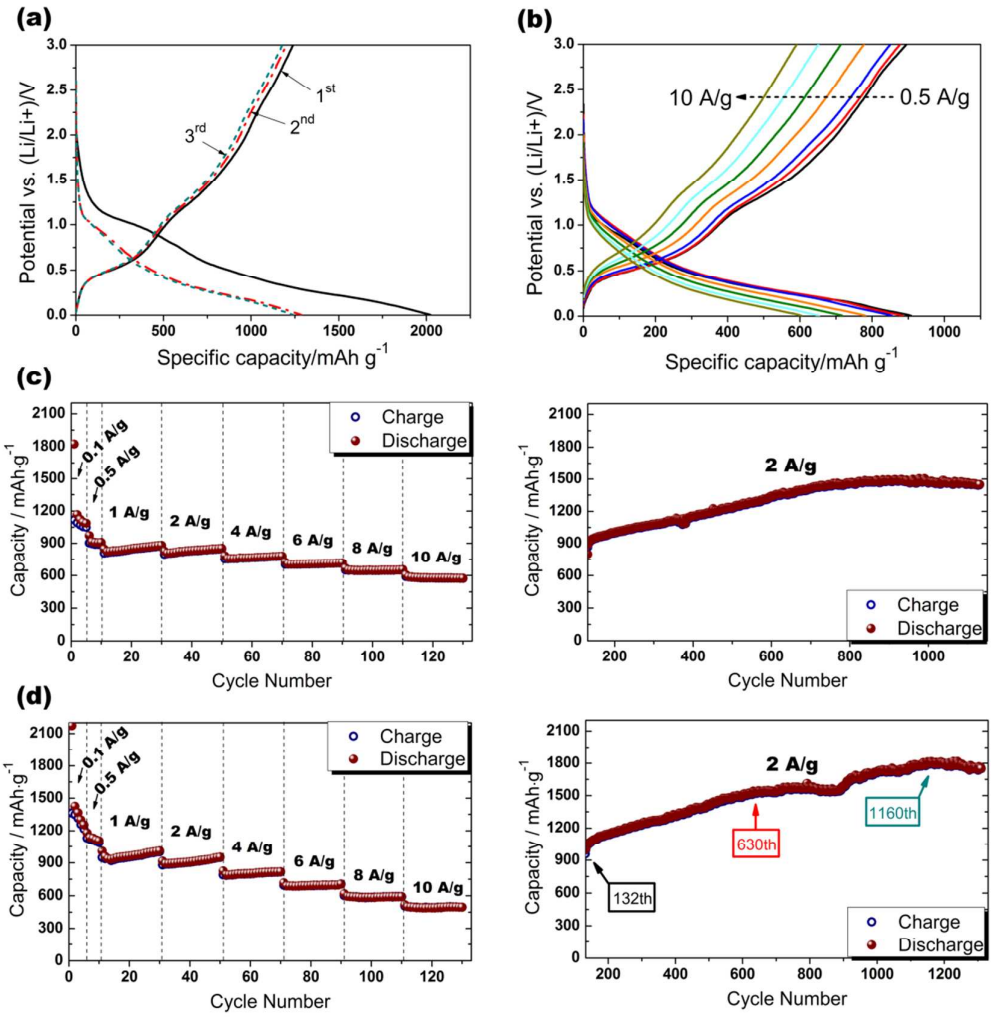

Figure 3. Electrochemical performances of SnO_2/G composite cycled between 0.005 – 3 V. Charge/discharge curves of SnO_2/G composite at (a) current density 0.1 $A \cdot g^{-1}$ and (b) higher rates, i.e. 0.5, 1, 2, 4, 6, 8, 10 $A \cdot g^{-1}$. Rate capability and subsequent cycling tests at 2 $A \cdot g^{-1}$ of (c) sample 1 and (d) sample 2.

To investigate the possible mechanisms behind such anomalous capacity achieved in SnO_2/G composites, dQ/dV plots in view of different stages of increment, together with TEM and ex-situ XRD on cycled electrode were shown in Figure 4. Figure 4a and 4b indicated the charge/discharge curves and corresponding dQ/dV plots of 132th, 630th, and 1160th cycles of SnO_2/G composite (corresponds to Figure 3d). The stable reduction peak at 0.2 V along with corresponding oxidation peak at 0.5 V strongly suggestd highly reversible alloying/dealloying reactions between Sn and Li without

any obvious capacity fade. The stable reversible capacity was attributed to the critical sizes of SnO_2 nanoparticles. Dahn et al. claimed that the particle size is one of the key factors for stable cycling performance of SnO_2, where smaller particle size could help to prevent gradual aggregation of Sn into large clusters.[30] Similarly, Kim et al. proved that ~3nm-sized SnO_2 has no aggregation upon cycling with cubic Sn formation, whereas particles with larger sizes are more vulnerable to aggregation into tetragonal Sn clusters.[31] In our case, according to ex-situ XRD results shown in Figure 4d, instead of tetragonal Sn, α-Sn (JCPDS 5-390) with cubic crystal structure was confirmed on the fully-charged state of electrode after 1310 cycles. In addition, no aggregation of Sn was observed in the TEM shown in Figure 4c. As a comparison, a composite anode material consisting larger SnO_2 particles (~ 200 nm) and graphene was synthesized with morphology shown in Figure S8A. The critical effect of ultra-small active SnO_2 was demonstrated by the much inferior electrochemical performances of large SnO_2/G composite as shown in Figure S8B. Besides, the reduction peak at 1.1 V and the corresponding oxidation peak at 1.2 V could still be observed, indicating that the reversibility of the conversion reaction of SnO_2 (equation 1).

Interestingly, increasing capacities upon cycling were observed for both of the tested samples (shown in 3c and 3d). dQ/dV plots and TEM image were used to study the possible mechanism of such interesting phenomenon. As shown in Figure 4a, the enclosed areas lower than 0.2 V gradually increased upon cycling, which was most likely to be related to incremental RGO lithiation.[32] Correspondingly, the enclosed areas during lithium deintercalation from 0.5 to 3.0 V also gradually rose, which could be ascribed to incremental RGO delithiation. Furthermore, as shown in Figure 4c, owing to the large volume changes of SnO_2 nanoparticles, mesopores were generated in graphene nanosheets after prolonged cycling process. The resulting porous graphene nanosheets with more edges were able to provide more activated sites for Li storage, thus further enhancing the overall capacity of SnO_2/G composite. Besides, the newly generated mesopores also facilitated the penetration of electrolyte, thus further enhancing the lithium ion conductivity within the composite electrode.[33]

Besides, the enhanced specific area of the electrode led to a higher interfacial area between electrode and electrolyte, resulting in a higher lithium ion flux across such interface, which is also beneficial for the overall electrochemical performances. Fan et al. claimed that the theoretical reversible capacity for porous graphene with more edges for Li storage could reach as high as 1965 $mAh \cdot g^{-1}$.[34] If the theoretical capacities for graphene and SnO_2 components could be regarded as 1965 and 1494 $mAh \cdot g^{-1}$ (theoretical capacity of SnO_2 taking both equation 1 and 2 to be fully reversible) respectively, it was reasonable to expect a reversible capacity as high as 1813 $mAh \cdot g^{-1}$ for SnO_2/G composite as observed in SnO_2/G composite. The electrochemical performances of SnO_2 nanoparticles encapsulated in hollow glucose-derived carbon beads have been studied in one of our early works.[35] However, without the incorporation of graphene, such composite only delivered 712 and 400 $mAh \cdot g^{-1}$ at current densities of 100 and 500 $mA \cdot g^{-1}$, respectively, showing much inferior performances comparing to SnO_2/G in this work. A stable Li_2CO_3 phase (JCPDS 22-1141) (Figure 4d) was identified after cycling by ex-situ XRD, which was normally recognized as a main component of electrolyte degradation products.[36] Besides, according to Figure S9, the average coulombic efficiencies from 131th to extending cycles for both samples (shown in 3c and 3d) were around 99.4 %. Such high coulombic efficiencies indicated the high reversibility of the charge/discharge process, including the reaction between SnO_2 and Li, and lithium storage on graphene surface.

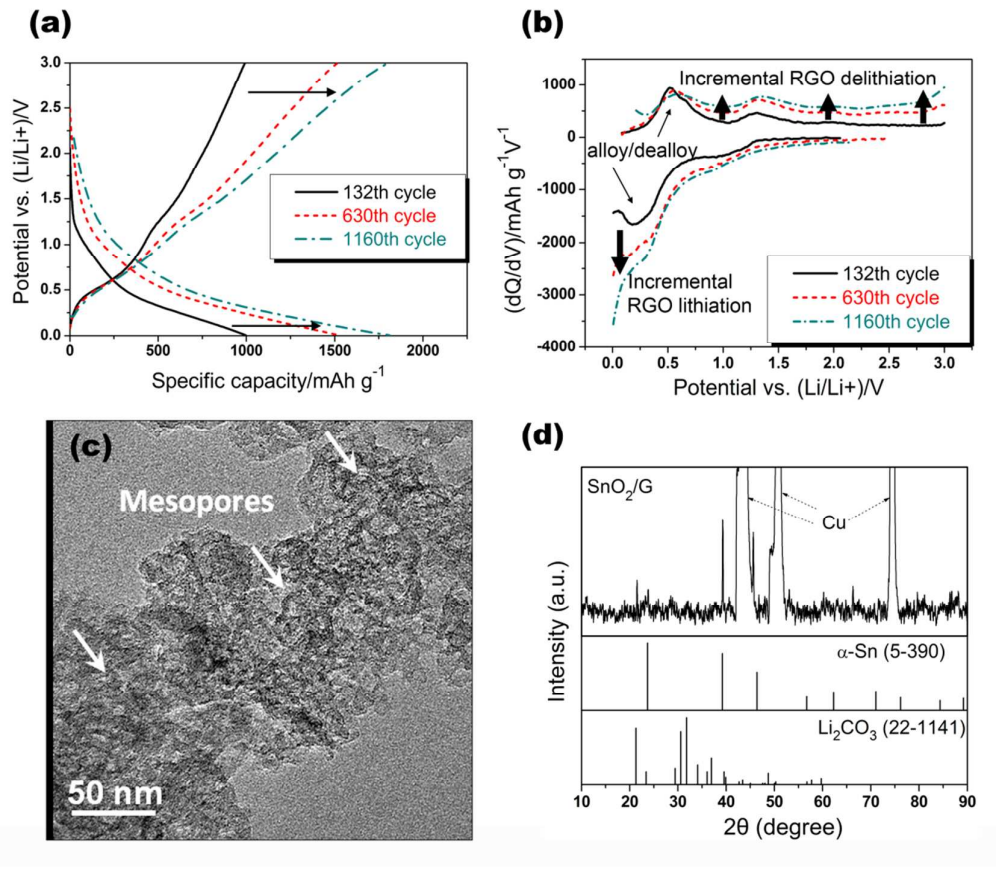

Figure 4. (a) Charge/discharge curves and (b) corresponding dQ/dV plots of different cycling stages. (c) Bright field TEM image and (d) ex-situ XRD pattern of SnO_2/G electrode (corresponding to Figure 3d) after 1310 cycles.

Conclusions

Ultra-small SnO_2 nanoparticles with an average diameter of 3 nm decorated on graphene nanosheets were successfully synthesized through a one-step hydrothermal method. This composite structure exhibited superior electrochemical performance as an anode material for LIBs, delivering 1239 mAh·g^{-1} initial charge capacity and 574 mAh·g^{-1} high rate capacity under the current densities of 0.1 and 10 A·g^{-1}, respectively. Most surprisingly, this anode material was capable of delivering an exceptionally high reversible capacity of 1813 mAh·g^{-1} under a current density of 2 A·g^{-1} after a steady increment throughout 1310 cycles. A high initial reversible capacity (1239 mAh·g^{-1}), excellent high rate performance (574 mAh·g^{-1} at 10 A·g^{-1}), and superior cycling

performance were achieved in the as-obtained SnO_2/G composite. With the aid of various experiments, possible mechanisms for such superior performance were proposed. 1) Ultra-small sizes of SnO_2 particles that partially initiated reversible conversion between SnO_2 and Li_2O upon cycling, and accommodated the volume changes during charge/discharge process. 2) Graphene network that not only enhanced the conductivity of the composite but also reversibly accommodated large amount of lithium. 3) Severe expansion/contraction of SnO_2 during lithiation/delithiation constructed graphene to be mesoporous with more activated sites for Li storage. 4) Polymeric gel-like film formation as a result of electrolyte decomposition contributed to extra capacity. These findings may enlighten the following works on exploring large reversible capacity on metal oxides, graphene, and their synergic composites as anodes for LIBs.

References

1. Goodenough, J. B.; Kim, Y., Challenges for Rechargeable Li Batteries†. *Chem. Mater.* **2009,** 22, (3), 587-603.

2. Armand, M.; Tarascon, J. M., Building better batteries. *Nature* **2008,** 451, (7179), 652-657.

3. Cabana, J.; Monconduit, L.; Larcher, D.; Palacín, M. R., Beyond Intercalation-Based Li-Ion Batteries: The State of the Art and Challenges of Electrode Materials Reacting Through Conversion Reactions. *Adv. Mater.* **2010,** 22, (35), E170-E192.

4. Chen, J. S.; Lou, X. W., SnO2-Based Nanomaterials: Synthesis and Application in Lithium-Ion Batteries. *Small* **2013**, n/a-n/a.

5. Idota, Y., Tin-Based Amorphous Oxide: A High-Capacity Lithium-Ion-Storage Material. *Science* **1997,** 276, (5317), 1395-1397.

6. Poizot, P.; Laruelle, S.; Grugeon, S.; Dupont, L.; Tarascon, J. M., Nano-sized transition-metal oxides as negative-electrode materials for lithium-ion batteries. *Nature* **2000,** 407, 496-499.

7. Chen, Y.; Song, B.; Lu, L.; Xue, J., Ultra-small Fe3O4 nanoparticle decorated graphene nanosheets with superior cyclic performance and rate capability. *Nanoscale* **2013,** 5, (15), 6797-6803.

8. Jeong, J.-M.; Choi, B. G.; Lee, S. C.; Lee, K. G.; Chang, S.-J.; Han, Y.-K.; Lee, Y. B.; Lee, H. U.; Kwon, S.; Lee, G.; Lee, C.-S.; Huh, Y. S., Hierarchical Hollow Spheres of Fe2O3@Polyaniline for Lithium Ion Battery Anodes. *Adv. Mater.* **2013**, n/a-n/a.

9. Gu, X.; Chen, L.; Ju, Z.; Xu, H.; Yang, J.; Qian, Y., Controlled Growth of Porous α-Fe2O3 Branches on β-MnO2 Nanorods for Excellent Performance in Lithium-Ion Batteries. *Adv. Funct. Mater.* **2013**.

10. Wang, Y.; Zhang, H. J.; Lu, L.; Stubbs, L. P.; Wong, C. C.; Lin, J., Designed Functional Systems from Peapod-like Co@Carbon to Co3O4@Carbon Nanocomposites. *ACS Nano* **2010,** 4, (8), 4753-4761.

11. Chen, Z.; Zhou, M.; Cao, Y.; Ai, X.; Yang, H.; Liu, J., In Situ Generation of Few-Layer Graphene Coatings on SnO2-SiC Core-Shell Nanoparticles for High-Performance Lithium-Ion Storage. *Advanced*

Energy Materials **2012,** 2, (1), 95-102.

12. Han, F.; Li, W.-C.; Li, M.-R.; Lu, A.-H., Fabrication of superior-performance SnO2@C composites for lithium-ion anodes using tubular mesoporous carbon with thin carbon walls and high pore volume. *J. Mater. Chem.* **2012,** 22, (19), 9645-9651.

13. Jiang, L.-Y.; Wu, X.-L.; Guo, Y.-G.; Wan, L.-J., SnO2-Based Hierarchical Nanomicrostructures: Facile Synthesis and Their Applications in Gas Sensors and Lithium-Ion Batteries. *The Journal of Physical Chemistry C* **2009,** 113, (32), 14213-14219.

14. Zhou, X.; Wan, L. J.; Guo, Y. G., Binding SnO2 nanocrystals in nitrogen-doped graphene sheets as anode materials for lithium-ion batteries. *Adv Mater* **2013,** 25, (15), 2152-7.

15. Guo, Y.-G.; Hu, J.-S.; Wan, L.-J., Nanostructured Materials for Electrochemical Energy Conversion and Storage Devices. *Adv. Mater.* **2008,** 20, (15), 2878-2887.

16. Bruce, P. G.; Scrosati, B.; Tarascon, J.-M., Nanomaterials for Rechargeable Lithium Batteries. *Angew. Chem. Int. Ed.* **2008,** 47, (16), 2930-2946.

17. Yang, S.; Yue, W.; Zhu, J.; Ren, Y.; Yang, X., Graphene-Based Mesoporous SnO2 with Enhanced Electrochemical Performance for Lithium-Ion Batteries. *Adv. Funct. Mater.* **2013**, n/a-n/a.

18. Lin, J.; Peng, Z.; Xiang, C.; Ruan, G.; Yan, Z.; Natelson, D.; Tour, J. M., Graphene Nanoribbon and Nanostructured SnO2 Composite Anodes for Lithium Ion Batteries. *ACS Nano* **2013**.

19. Zhang, X.; Wang, B.; Sunarso, J.; Liu, S.; Zhi, L., Graphene nanostructures toward clean energy technology applications. *Wiley Interdisciplinary Reviews: Energy and Environment* **2012,** 1, (3), 317-336.

20. Wang, X.; Cao, X.; Bourgeois, L.; Guan, H.; Chen, S.; Zhong, Y.; Tang, D.-M.; Li, H.; Zhai, T.; Li, L.; Bando, Y.; Golberg, D., N-Doped Graphene-SnO2 Sandwich Paper for High-Performance Lithium-Ion Batteries. *Adv. Funct. Mater.* **2012,** 22, (13), 2682-2690.

21. Huang, X.; Zhou, X.; Zhou, L.; Qian, K.; Wang, Y.; Liu, Z.; Yu, C., A Facile One-Step Solvothermal Synthesis of SnO2/Graphene Nanocomposite and Its Application as an Anode Material for Lithium-Ion Batteries. *ChemPhysChem* **2011,** 12, (2), 278-281.

22. Pei, S.; Cheng, H.-M., The reduction of graphene oxide. *Carbon* **2012,** 50, (9), 3210-3228.

23. Demir-Cakan, R.; Hu, Y. S.; Antonietti, M.; Maier, J.; Titirici, M. M., Facile one-pot synthesis of mesoporous SnO2 microspheres via nanoparticles assembly and lithium storage properties. *Chem Mater* **2008,** 20, (4), 1227-1229.

24. Jiang, L. Y.; Wu, X. L.; Guo, Y. G.; Wan, L. J., SnO2-Based Hierarchical Nanomicrostructures: Facile Synthesis and Their Applications in Gas Sensors and Lithium-Ion Batteries. *J Phys Chem C* **2009,** 113, (32), 14213-14219.

25. Yang, S. B.; Feng, X. L.; Ivanovici, S.; Mullen, K., Fabrication of Graphene-Encapsulated Oxide Nanoparticles: Towards High-Performance Anode Materials for Lithium Storage. *Angew Chem Int Edit* **2010,** 49, (45), 8408-8411.

26. Han, F.; Li, W. C.; Li, M. R.; Lu, A. H., Fabrication of superior-performance SnO2@C composites for lithium-ion anodes using tubular mesoporous carbon with thin carbon walls and high pore volume. *J Mater Chem* **2012,** 22, (19), 9645-9651.

27. Li, J. X.; Zhao, Y.; Wang, N.; Guan, L. H., A high performance carrier for SnO2 nanoparticles used in lithium ion battery. *Chem Commun* **2011,** 47, (18), 5238-5240.

28. Courtney, I. A.; McKinnon, W. R.; Dahn, J. R., On the aggregation of tin in SnO composite glasses caused by the reversible reaction with lithium. *J Electrochem Soc* **1999,** 146, (1), 59-68.

29. Chang, S. T.; Leu, I. C.; Liao, C. L.; Yen, J. H.; Hon, M. H., Electrochemical behavior of

nanocrystalline tin oxide electrodeposited on a Cu substrate for Li-ion batteries. *J Mater Chem* **2004,** 14, (12), 1821-1826.

30. Courtney, I. A.; Dahn, J. R., Key factors controlling the reversibility of the reaction of lithium with SnO2 and Sn2BPO6 glass. *J Electrochem Soc* **1997,** 144, (9), 2943-2948.

31. Kim, C.; Noh, M.; Choi, M.; Cho, J.; Park, B., Critical size of a nano SnO2 electrode for Li-secondary battery. *Chem Mater* **2005,** 17, (12), 3297-3301.

32. Chockla, A. M.; Panthani, M. G.; Holmberg, V. C.; Hessel, C. M.; Reid, D. K.; Bogart, T. D.; Harris, J. T.; Mullins, C. B.; Korgel, B. A., Electrochemical Lithiation of Graphene-Supported Silicon and Germanium for Rechargeable Batteries. *J Phys Chem C* **2012,** 116, (22), 11917-11923.

33. Hu, L.; Tang, Z.; Zhang, Z., New composite polymer electrolyte comprising mesoporous lithium aluminate nanosheets and PEO/LiClO4. *J. Power Sources* **2007,** 166, (1), 226-232.

34. Fan, Z. J.; Yan, J.; Ning, G. Q.; Wei, T.; Zhi, L. J.; Wei, F., Porous graphene networks as high performance anode materials for lithium ion batteries. *Carbon* **2013,** 60, 558-561.

35. Chen, Y.; Huang, Q. Z.; Wang, J.; Wang, Q.; Xue, J. M., Synthesis of monodispersed SnO2@C composite hollow spheres for lithium ion battery anode applications. *J. Mater. Chem.* **2011,** 21, (43), 17448.

36. Aurbach, D., Review of selected electrode-solution interactions which determine the performance of Li and Li ion batteries. *J Power Sources* **2000,** 89, (2), 206-218.